

## Angle-resolved-photoemission study of the Cr(110) surface and of antiferro- to paramagnetic phase transition

L. I. Johansson\*

*Stanford Synchrotron Radiation Laboratory, Stanford, California 94305*

L.-G. Petersson and K.-F. Berggren

*Department of Physics and Measurement Technology, Linköping University, S-581 83 Linköping, Sweden*

J. W. Allen

*Xerox Palo Alto Research Center, Palo Alto, California 94304*

(Received 21 March 1980)

Angle-resolved-photoemission measurements were performed on the Cr(110) surface at temperatures below and above the Néel temperature. The results are compared with previously calculated band structures, and for the antiferromagnetic phase fairly good agreement is obtained assuming direct transitions. Differences observed in photoemission spectra recorded below and above the Néel temperature are discussed in terms of the magnetic phase transition. For the paramagnetic phase the results could not be fully accounted for by calculated bulk band structures; possible explanations of the observed discrepancies are discussed.

### I. INTRODUCTION

The purpose of the present investigation is twofold. First we want to investigate the electronic band structure of chromium, using angle-resolved photoemission, and compare our results with calculated band structures. Secondly we want to try to determine effects on the electron band structure caused by the antiferro- to paramagnetic phase transition,<sup>1</sup> which occurs at a Néel temperature of  $T_N = 312$  K.

Rather few photoemission experiments have been carried out on Cr so far,<sup>2-5</sup> and none of them has been an angle-resolved study for mapping out the energy bands. This is in a way remarkable since Cr appears to be unique among metals in that an itinerant electron antiferromagnetic state is formed below the Néel temperature. More experimental knowledge about the occupied part of the electron band structure of Cr is consequently called for at least in order to assess the accuracy of calculated results.<sup>6-10</sup> The angle-resolved-photoemission technique is well suited for obtaining such information.<sup>11</sup> Even more interesting, however, would be to observe effects on the band structure caused by the magnetic phase transition. In transforming from the para- to the antiferromagnetic phase, energy gaps appear at the Fermi level, at certain points in the Brillouin zone, due to band hybridization.<sup>6</sup> The existence of these gaps in the antiferromagnetic phase has been verified in optical experiments.<sup>12,13</sup> The gaps are small ( $\leq 0.2$  eV), and the changes in the band structure indicate

that the effects likely to be seen in photoemission spectra will be rather small; nevertheless, if observed, they would be most interesting. For the above reasons we have carried out an angle-resolved-photoemission study of a Cr(110) surface. Normal emission from this surface corresponds to the  $\Gamma \rightarrow N$  direction in  $\bar{k}$  space, along which prominent antiferromagnetic gaps are expected. Measurements have been performed at temperatures both below and above the Néel temperature.

For the main purpose of revealing emission from surface induced states, controlled exposures of oxygen to the clean surface were carried out. Some data on the initial oxidation of the Cr(110) surface is therefore also presented.

### II. EXPERIMENTAL

The experiments were performed on the 8° line of Beam Line I at Stanford Synchrotron Radiation Laboratory. Linearly polarized radiation is obtained from this line (polarized in the horizontal plane). The angle resolved photoemission experiments were carried out utilizing a Vacuum Generators ADES 400 system. It contains an electron energy analyzer that can be rotated around the sample in the horizontal plane. Most of our data were collected for normal electron emission ( $\theta_e = 0^\circ$ ) at incidence angles of the photon beam of 15° and 75°, relative to the sample surface normal. The energy resolution of the energy

analyzer, which has an acceptance angle of  $\pm 2^\circ$ , was kept at 0.18 eV in the present measurements. The base pressure of the instrument was  $\leq 8 \times 10^{-11}$  torr and the working pressure during the measurements was  $\leq 2 \times 10^{-10}$  torr.

A sample having the desired orientation within  $2^\circ$  was obtained from a single crystal by cutting with a diamond saw. After mechanical polishing the surface was polished electrolytically in a perchloric and acetic acid solution. The sample was then cleaned *in situ* by repeated sputter-anneal cycles. Sputtering was performed using Ar ions of energies between 2.0–0.5 keV. Annealing was performed at 600°C, which was the highest temperature at which our sample holder allowed us to anneal. The cleanliness of the sample was checked by Auger electron spectroscopy. In order to get a carbon free surface we found that we had to complement the sputter-anneal cycles with small oxygen exposures during a few annealings ( $\sim 10^{-7}$  torr of oxygen during annealings of a few minutes) to burn off the carbon. The surface geometry was checked using low-energy electron diffraction (LEED). The characteristic pattern was observed although the spots were a little blurry and not very intense. After the experiment the surface geometry was checked again in a SEM (scanning electron microscope) and a good channeling pattern was observed. From these checks we conclude that the surface was of sufficient quality to represent clean and ordered Cr(110).

A cold finger had been attached to the system in such a way that the sample could be cooled as well as heated. The temperature was measured with a thermocouple that was spot welded to the side of the crystal.

### III. EXPERIMENTAL RESULTS AND DISCUSSION

Electron energy distribution curves (EDC's) obtained at normal electron emission for different photon energies from Cr(110) are shown in Fig. 1. For the spectra in Fig. 1(a) the photon beam was incident at an angle of  $15^\circ$ , relative to the surface normal while for the spectra in Fig. 1(b) the angle was  $75^\circ$ . The spectra are plotted against the initial electron energy with the Fermi level chosen as  $E_F = 0$  eV. These spectra were recorded at a temperature of 230 K and represent consequently the antiferromagnetic phase of Cr.

The characteristic features of these spectra are:

- (1) A structure just below the Fermi level which is clearly observed in the spectra taken at  $\alpha = 15^\circ$ .
- (2) A main peak at about 1 eV below  $E_F$  which shows some dispersion especially at the low photon energies.
- (3) and (4) Two broad structures, around 3 and 6 eV below  $E_F$ , respectively, which do not show appreciable

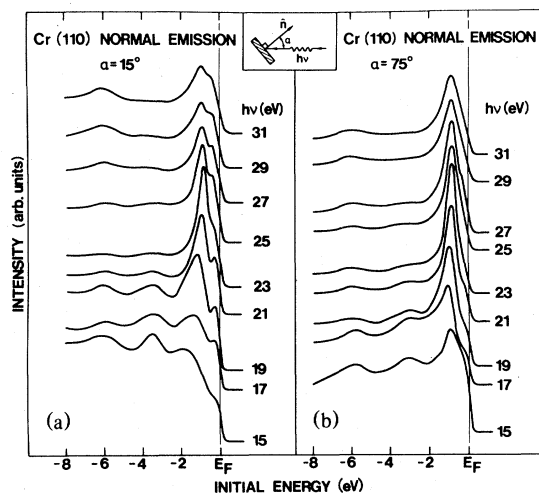


FIG. 1. EDC's recorded at normal electron emission from Cr(110) and at a temperature of 230 K for (a)  $\alpha = 15^\circ$  and (b)  $\alpha = 75^\circ$ .

able dispersion but becomes weaker at the higher photon energies.

In the comparison with calculated band structures we will concentrate on the first three spectral features and the 6-eV peak will be discussed later.

The electron band structure of Cr in the antiferromagnetic phase was first calculated by Asano and Yamashita<sup>6</sup> (YA). They applied a Green's-function method and calculated the band structure for the perfect antiferromagnetic state; i.e., they assumed a spin superstructure determined by a spin-density wave commensurate with the lattice. In pure Cr the spin-density wave has a wave vector that is  $0.95 (2\pi/a)$ , which is fairly close to the assumed commensurate value of  $(2\pi/a)$ , where  $a$  is the lattice constant. The crystal structure for the antiferromagnetic state is the CsCl structure. This means that the crystal symmetry is lower in the antiferromagnetic than in the paramagnetic phase, which has a bcc crystal structure. The calculated results<sup>6</sup> for the antiferromagnetic phase along the  $\langle 110 \rangle$  direction are shown in Fig. 2. Also shown in Fig. 2 are our experimental results, assuming a final state with a free-electronlike dispersion of  $E = \hbar^2 k^2 / 2m + V_0 + \Phi$ , where  $V_0$  is the inner potential,  $\Phi$  the work function, and  $E$  the energy above  $E_F$ . As discussed below a value of  $V_0 + \Phi = -5.2$  eV has been used in this analysis. The dots represent data taken at  $\alpha = 15^\circ$  and the crosses data taken at  $\alpha = 75^\circ$ . The vertical bars indicate the estimated uncertainty in the determination of the peak positions for the cases where it is larger than 0.1 eV.

The structure just below the Fermi level in the spectra taken at  $\alpha = 15^\circ$  is interpreted as originating

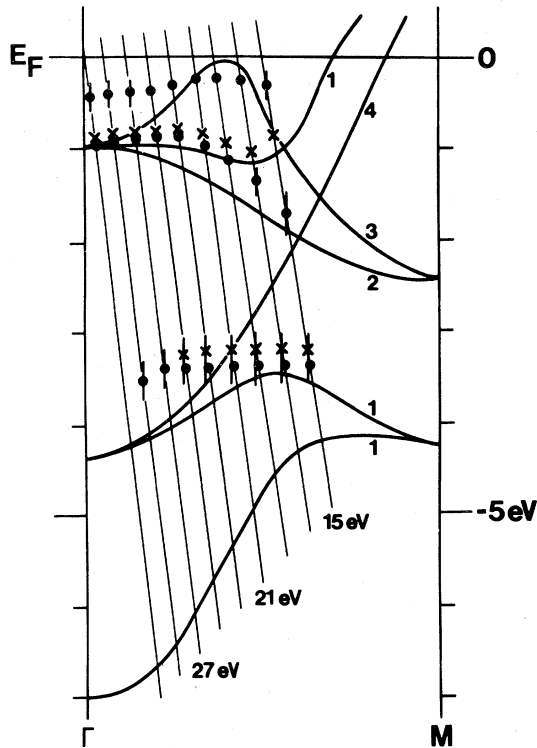


FIG. 2. Calculated (Ref. 6) band structure for the antiferromagnetic phase along the  $\langle 110 \rangle$  direction and our experimental results when assuming direct transitions and a free-electronlike final state. The dots represent data obtained at  $\alpha = 15^\circ$  and the crosses, data obtained at  $\alpha = 75^\circ$ .

from transitions from the  $\Sigma_3$  band. The main peak in the spectra taken at  $\alpha = 75^\circ$  we associate with transitions from the  $\Sigma_1$  band while the main peak in the spectra taken at  $\alpha = 15^\circ$  is associated with transitions predominantly from the  $\Sigma_2$  band. The broad structure between 3 and 4 eV below  $E_F$ , for which the uncertainty in peak position determination is quite large, is interpreted as arising from the  $\Sigma_1$  and possibly the  $\Sigma_4$  band. Most of the structure observed can, as seen in Fig. 2, be accounted for by direct transitions to a free-electronlike final state. With these assignments, the polarization effects observed are consistent with symmetry selection rules.<sup>14</sup> At normal electron emission and pure  $p$ -polarized light ( $\alpha = 90^\circ$ ) only  $\Sigma_1$  initial states are allowed. The  $\Sigma_3$  band close to the Fermi level should thus not be observed in spectra taken at such a geometry. For purely  $s$ -polarized light ( $\alpha = 0^\circ$ ) only initial states of  $\Sigma_3$  symmetry would be allowed if the electric field vector were along the  $\langle 100 \rangle$  axis, and only  $\Sigma_4$  initial states would be allowed if it were along the  $\langle 1\bar{1}0 \rangle$  axis. Unfortunately, experimental circumstances precluded aligning the crystal so that the electric field vector was along the  $\langle 100 \rangle$  axis at normal light incidence ( $\alpha = 0^\circ$ ). From

our LEED pattern we estimate an angle of about  $35^\circ$  between the electric vector and the  $\langle 100 \rangle$  axis. Although we consequently were not aligned for obtaining maximal sensitivity for  $\Sigma_3$  initial states we do, however, observe an enhanced emission from  $\Sigma_3$  initial states when decreasing  $\alpha$  from  $75^\circ$  to  $15^\circ$  as expected. We note that no emission should be observed<sup>14</sup> from the  $\Sigma_2$  band at normal electron emission. The symmetry selection rules<sup>14</sup> apply, however, strictly only when using an analyzer with a vanishingly small acceptance solid angle. The acceptance angle of  $\pm 2^\circ$  of the analyzer used therefore permits electrons excited from the  $\Sigma_2$  band to be observed.

The dispersion of the main peaks in Fig. 1 reflects fairly well the trends of the calculated bands shown in Fig. 2, although the experimental values are somewhat smaller than the calculated ones about 0.1–0.2 eV. The position of the structure observed close to  $E_F$  agrees fairly well with the position of the calculated  $\Sigma_3$  bulk band for photon energies between 15 and 23 eV, but for larger photon energies a discrepancy is observed. This may be due to that spin-orbit interactions were neglected in the band-structure calculation. Spin-orbit interactions would have the effect of creating a gap, of the order of a few tenths of an eV, between the  $\Sigma_3$  band and the degenerate  $\Sigma_1$  and  $\Sigma_2$  bands at  $\Gamma$  (at the  $\Gamma'_{25}$  point shown in Fig. 3).

Although this might explain the discrepancy we prefer in the following to rely on the calculated band structure and to look for other explanations. The other alternatives then are that this structure is due to a surface state (or resonance) or due to a more complicated final-state band. The latter alternative will be discussed first.

The result of a Hartree band-structure calculation<sup>8</sup> along the  $\langle 110 \rangle$  direction  $\Gamma \rightarrow N$ , for paramagnetic Cr is shown in Fig. 3 (solid lines). At energies above  $E_F$  only bands of  $\Sigma_1$  symmetry are shown since they constitute the only allowed final-state bands at normal electron emission. A gross picture of the band structure for the antiferromagnetic state in Cr is obtained when the calculated bands along the  $N \rightarrow H$  direction are folded back into the band structure along the  $\langle 110 \rangle$  direction (dashed lines). The correspondence between directions in the first Brillouin zone of a bcc structure with that of a CsCl structure are shown in Fig. 4. The hybridization giving rise to the energy gap at the Fermi level occurs between the two  $\Sigma_3$  bands (the solid and dashed bands crossing  $E_F$ ). The dotted curve represents our assumed free-electronlike final-state band,  $E = \hbar^2 k^2 / 2m - 5.2$  eV. The value  $V_0 + \Phi = -5.2$  eV that has been used was the result of a fit of this band to the calculated  $\Sigma_1$  band for energies between 15 and 25 eV. This seemed to us the most reasonable choice since neither a band structure for the antiferromagnetic phase describing final states with energies between 15 and 35 eV nor accurate values for  $V_0$  and  $\Phi$  has been published. The free-



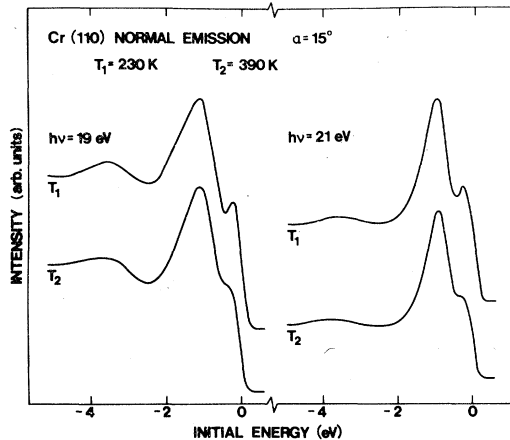


FIG. 5. EDC's recorded at normal electron emission from Cr(110), for  $\alpha = 15^\circ$ , and at temperatures below and above the Néel temperature  $T_N = 312$  K.

plained by pure temperature broadening effects.<sup>15</sup> Therefore we interpret the results shown in Fig. 5 as a direct spectroscopic observation of changes induced in the electronic band structure by the magnetic phase transition.

In order to visualize the changes induced in the density of states by the magnetic phase transition, model bands were generated and the one-dimensional density of states calculated for simulated para- and antiferromagnetic band structures. The results are shown in Fig. 6 where, for the simulated antiferromagnetic band structure, a distinct peak is seen to appear in the density of states between  $E_F$  and the main peak.

In comparing Figs. 2 and 3 there are some differences that we so far have not mentioned. The  $N'_1$  point is in Fig. 3 located below  $E_F$  (at about  $-1$  eV) while this point is about  $1$  eV above  $E_F$  in all other calculations<sup>6-10</sup> and is moreover shown to be very little affected by the phase transition in the YA calculation. The width of the occupied bands ( $E_F - \Gamma_1$  energy separation) does vary among the different calculated results by as much as 40%. YA (Fig. 2) gives the smallest width ( $\sim 7$  eV) while Fry *et al.*<sup>8</sup> (Fig. 3) give the largest width ( $\sim 9.7$  eV). These variations probably depend on the way exchange effects are treated in the calculations. Our experimental results agree best with the YA results.

Ideally the structure at the Fermi level should disappear completely in the spectra recorded at photon energies below about 20 eV (see Figs. 2 and 3) when going from the antiferromagnetic to the paramagnetic phase. That it does not disappear may be due to several reasons. The Néel temperature of the surface layer may be different than that of the bulk.<sup>16</sup> One may also speculate that dynamic magnetic fluctuations giving rise to short-range ordering ef-

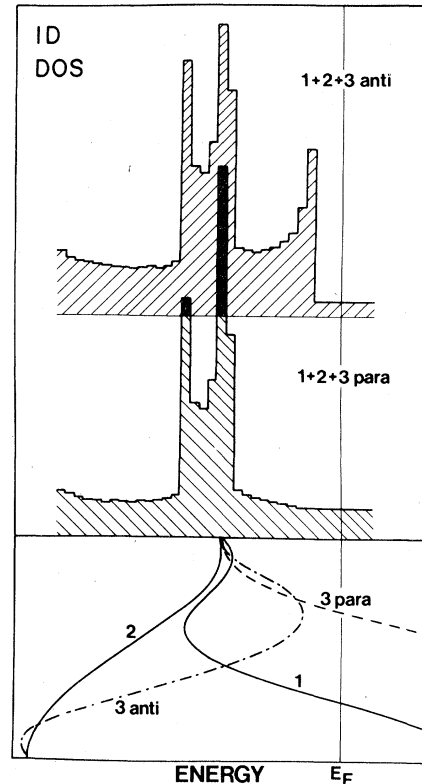


FIG. 6. In the lower part of the figure model bands generated to simulate the electronic band structure of the paramagnetic phase (band 1 + 2 + 3 para) and of the antiferromagnetic phase (band 1 + 2 + 3 anti) are shown. Assuming the same degeneracy in the four bands the one-dimensional density of states (DOS) shown by the histograms are obtained for the two phases. If the effect discussed in the text of spin-orbit interactions was simulated, the DOS of the paramagnetic phase would also show some more weight close to the Fermi level.

fects may occur above the Néel temperature so that a simple paramagnetic state is not immediately created at temperatures higher than the Néel point. Earlier measurements<sup>17</sup> using inelastic magnetic scattering of neutrons have been interpreted in terms of spin-wavelike excitations, which persist far into the paramagnetic phase, i.e., up to  $T \sim 1.5T_N$ . Also resistive anomalies<sup>18</sup> indicate the appearance of an additional scattering mechanism in the form of spin correlations long before the actual magnetic transition is reached from above (also here  $T \lesssim 1.5T_N$ ). This type of fluctuation phenomenon is also consistent with more recent discussions of (ferro)magnetism.<sup>19</sup> Finally surface induced states<sup>20</sup> may also appear and interfere with the contribution from bulk states.

Investigations of other transition-metal surfaces<sup>21, 22</sup> have provided strong evidence of surface effects and calculations have been carried out<sup>23, 24</sup> verifying the existence of localized surface states or resonances on

such surfaces. In the antiferromagnetic phase, where hybridization gaps are opened up at the Fermi level, surface states are likely to be created.<sup>25,26</sup> The assignment of surface induced states to structures in a photoemission spectrum is commonly inferred from their sensitivity to surface contamination and their insensitivity to variations of photon energy. The structure observed just below  $E_F$  in the spectra taken at temperatures above  $T_N$  but also in the spectra recorded for the antiferromagnetic phase at photon energies greater than 25 eV meets the second criterion. Therefore the first criterion was also tested by studying the effects of controlled exposures of oxygen. The result of this test was negative in the sense that the structure was not found to be sensitive to surface contamination. The typical effects observed are illustrated in Fig. 7 where EDC's recorded at room temperature and at oxygen exposures of 0, 1, and 2 L (1 L =  $10^{-6}$  torr sec) are shown. The structure at the Fermi level is not found to be attenuated more than the structure assigned to direct band transitions. The main effect observed is the appearance of a broad peak around 5.5 eV below  $E_F$  which originates from O 2p states. None of the structures discussed previously can conclusively be attributed to surface induced states.

The structure seen around 6 eV below  $E_F$  in all our Cr(110) spectra (see Fig. 2) is not ascribed to residual surface contamination. This structure was recently also observed<sup>4</sup> for evaporated Cr films and a similar structure has been observed in photoemission spectra from other transition metals<sup>27</sup> and has been interpret-

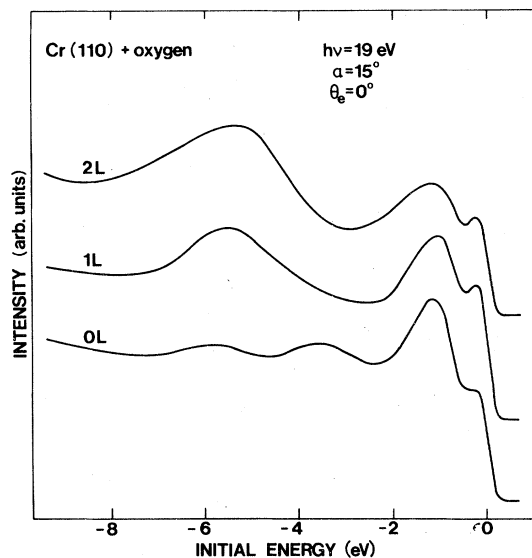


FIG. 7. EDC's recorded at normal emission and at  $\alpha = 15^\circ$  from Cr(110) after different oxygen exposures at room temperature.

ed as arising from photoionization processes involving more than one electron.

The broad structureless oxygen-derived peak obtained after oxygen exposures performed at room temperature has previously been interpreted,<sup>2</sup> when combined with other experimental data, as indicating formation of an amorphous oxide layer. Heat treatments after oxygen exposures at room temperature have previously been found, in LEED experiments,<sup>2,3,28</sup> to produce an ordered structure, probably corresponding to a crystalline chromium oxide phase. The effect on the oxygen-derived peak upon heating is illustrated by the spectra shown in Fig. 8 which were recorded at room temperature. Curve 1 represents the clean surface while curve 2 is recorded after an oxygen exposure of 2 L performed at room temperature. Heating to 500°C for 3 min then produced curve 3 where the O 2p-derived structure is seen to be split into two peaks, located around 5 and 7 eV below  $E_F$ , respectively. Curves 1, 2, and 3 were recorded at normal electron emission ( $\theta_e = 0^\circ$ ), while curves 4 and 5 were recorded at a polar angle of  $15^\circ$ . Curve 5 was collected before and curve 4 after the heating but both at an exposure of 2 L. No change with polar angle of the O 2p structure is observed before the heating (compare 2 and 5) which is consistent with a disordered oxygen configuration as in an amorphous layer. Upon heating the O 2p peak splits into two peaks which indicates the formation of

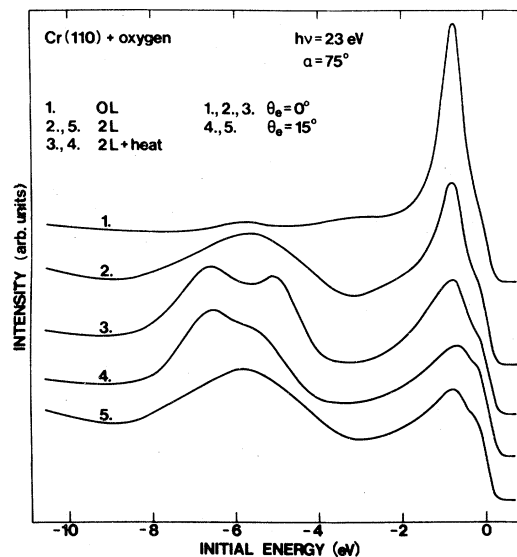


FIG. 8. EDC's recorded at  $\alpha = 75^\circ$  from Cr(110) after different oxygen exposures performed at room temperature. Curve 1 represents 0 L and  $\theta_e = 0^\circ$ ; curve 2 2 L and  $\theta_e = 0^\circ$ ; curve 3 2 L plus heating to 500°C for 3 min and  $\theta_e = 0^\circ$ ; curve 4 2 L plus heating to 500°C for 3 min and  $\theta_e = 15^\circ$ ; and curve 5 2 L and  $\theta_e = 15^\circ$ .

definite oxide bonds. A distinct change in the relative strength of these two O 2*p* peaks is observed upon a polar angle variation of 15° (compare curves 3 and 4) which indicates the presence of an ordered oxygen configuration. The sensitivity of the peak at about 5 eV below  $E_F$  to a polar angle change of 15° suggests that this peak originates predominantly from O 2*p* states of  $p_z$  character.

#### IV. SUMMARY

Most of the structures observed in the photoemission spectra recorded on the Cr(110) surface can be interpreted in terms of direct transitions from bulk bands to a free-electronlike final state. Our experimental results agree fairly well with Asano and Yamashita's<sup>6</sup> calculated band structure for the antiferromagnetic phase. Effects interpreted as induced by the antiferro- to paramagnetic phase transition on the electron band structure have been observed. The results obtained for the paramagnetic phase, i.e., at a temperature of 390 K, cannot, however, be fully accounted for by bulk band transitions using the calculated band structure for the paramagnetic phase. None of the observed structures could, using the commonly applied criteria, be attributed to emission from surface induced states. Our results suggest either that the Néel temperature of the surface is larger than the bulk value or that short-range ordering effects (spin correlations) remain above the Néel point, i.e., at the temperature of 390 K for which the experiments were carried out. The latter conjecture is con-

sistent with strong dynamic fluctuation phenomena observed previously in connection with inelastic scattering of neutrons<sup>17</sup> and with resistive anomalies.<sup>18</sup> In particular, the neutron scattering experiments have shown that there is no dramatic change in passing through  $T_N$ , which is in obvious agreement with present results. The interpretation involving fluctuations or, equivalently, short-range spin ordering above  $T_N$  is consequently a very strong candidate. If correct, the present work is the first demonstration of this phenomenon in an itinerant antiferromagnet by means of angle resolved photoemission. Finally this investigation has shown the feasibility of exploring effects on the band structure caused by the antiferro- to paramagnetic phase transition in Cr and by optimizing the experimental geometry, these effects could be explored in more detail.

#### ACKNOWLEDGMENTS

Two of us (L. I. J. and J. A.) gratefully acknowledge discussions with C. Herring. We would also like to thank J. L. Fry for helpful correspondence about the unoccupied part of the band structure of Cr and H. Skriver for informative discussions. The experiments were performed at the Stanford Synchrotron Radiation Laboratory which is supported by the National Science Foundation under Contract No. DMR 77-27489 in cooperation with the Stanford Linear Accelerator Center and the Department of Energy. Financial support from the Swedish National Science Research Council is also gratefully acknowledged.

\*Present address: Department of Phys. and Measurement Technology Linköping University, S-581 83 Linköping, Sweden.

<sup>1</sup>C. Herring, in *Magnetism*, edited by G. T. Rado and H. Suhl (Academic, New York, 1966), Vol. 4.

<sup>2</sup>G. Gewinner, J. C. Peruchetti, A. Jaegle, and A. Kalf, *Surf. Sci.* **78**, 439 (1978).

<sup>3</sup>J. C. Peruchetti, G. Gewinner, and A. Jaegle, *Surf. Sci.* **88**, 479 (1979).

<sup>4</sup>J. Barth, F. Gerken, K. L. I. Kobayashi, J. H. Weaver, and B. Sonntag, DESY Report No. SR-79/27 (unpublished).

<sup>5</sup>G. Gewinner, J. C. Peruchetti, A. Jaegle, and R. Riedinger, *Phys. Rev. Lett.* **43**, 935 (1979).

<sup>6</sup>S. Asano and J. Yamashita, *J. Phys. Soc. Jpn.* **23**, 714 (1967).

<sup>7</sup>J. Rath and J. Callaway, *Phys. Rev. B* **8**, 5398 (1973).

<sup>8</sup>J. L. Fry, N. E. Breuer, J. L. Thompson, and P. H. Dickinson, *Phys. Rev. B* **21**, 384 (1980); and (private communication).

<sup>9</sup>J. Kübler, *J. Magn. Magn. Mater.* (in press).

<sup>10</sup>H. Skriver has recently calculated the band structure for the antiferromagnetic state by means of the spin-polarized

local-density formalism. Relativistic effects except spin-orbit interactions are included. Skriver's results are in close agreement with the results in Ref. 6 [(private communication) and (unpublished)].

<sup>11</sup>See, for example, the results on Ni; F. J. Himpsel, J. A. Knapp, and D. A. Eastman, *Phys. Rev. B* **19**, 2919 (1979).

<sup>12</sup>A. S. Barker, Jr., B. T. Halperin, and T. M. Rice, *Phys. Rev. Lett.* **20**, 384 (1968).

<sup>13</sup>A. S. Barker, Jr., and J. A. Ditzemberger, *Phys. Rev. B* **11**, 4378 (1970).

<sup>14</sup>J. Hermanson, *Solid State Commun.* **22**, 9 (1977).

<sup>15</sup>N. J. Shevchik, *Phys. Rev. B* **16**, 3428 (1977). An increase in temperature from  $T_1 = 230$  K to  $T_2 = 390$  K yield for Cr, using Shevchik's model and  $\Delta k = \sqrt{22}\pi/a$  ( $a = 2.88$  Å in Cr), an energy broadening of

$$\Delta E(T_2) - \Delta E(T_1)$$

$$= 2\pi \Delta k [(k_B/M_A) \ln 2]^{1/2} (\sqrt{T_2} - \sqrt{T_1}) \approx 2 \times 10^{-3} \text{ eV}$$

and a decrease in the Debye-Waller factor

$\exp(-\Delta k^2 \langle u^2 \rangle)$  from 0.985 to 0.974. Thus  $k$  conservation is very little affected by this temperature increase, and the energy broadening is in our case about one percent of the instrumental resolution.

<sup>16</sup>It has been discussed that the surface, as well as defects or strain, may induce effects which increase the Néel temperature. See, for example, Y. Teraoka and J. Kanamori, in *Transition metals 1977*, edited by M. J. G. Lee, J. M. Perz, and E. Fawcett (Adlard and Son Ltd., Dorking, 1978), and references therein. The Néel temperature is known to be sensitive to the nesting, see Fig. 19 in Ref. 12, so it would be very interesting to compare our results to the results obtained on a doped crystal.

<sup>17</sup>J. Als-Nielsen and O. W. Dietrich, *Phys. Rev. Lett.* **22**, 290 (1969).

<sup>18</sup>C. H. Chiu, M. H. Jericho, and R. H. March, *Can. J. Phys.* **49**, 3010 (1971).

<sup>19</sup>J. Hubbard, *Phys. Rev. B* **19**, 2626 (1979), and references therein.

<sup>20</sup>M. Tomasek and S. Pich, *Phys. Status Solidi B* **89**, 11 (1978).

<sup>21</sup>B. Feuerbacher and B. Fitton, *Phys. Rev. Lett.* **29**, 786 (1972).

<sup>22</sup>R. C. Cinti, E. Al Khoury, B. K. Chakraverty, and N. E. Christensen, *Phys. Rev. B* **14**, 3295 (1976).

<sup>23</sup>M. Kawajivi, J. Hermanson, and W. Schwalm, *Solid State Commun.* **25**, 303 (1978).

<sup>24</sup>D. G. Dempsey, L. Kleinman, and E. Caruthers, *Phys. Rev. B* **13**, 1489 (1976).

<sup>25</sup>J. B. Pendry and S. J. Gurman, *Surf. Sci.* **49**, 87 (1975).

<sup>26</sup>G. Allen, *Surf. Sci.* **74**, 79 (1978).

<sup>27</sup>C. Guillot, Y. Ballu, J. Paigne, J. Lecante, K. P. Jain, P. Thiry, R. Pinchaux, Y. Petroff, and L. M. Falicov, *Phys. Rev. Lett.* **39**, 1632 (1977).

<sup>28</sup>P. Michel and Ch. Jardin, *Surf. Sci.* **36**, 478 (1973).